



Morphological Feature Description Method of Structural Surface in Borehole Image During In-Situ Instrumentation

Xianjian Zou^{1,5} · Chuanying Wang¹ · Yiteng Wang^{1,4} · Huan Song^{2,3}

Received: 18 July 2019 / Accepted: 18 February 2020 / Published online: 21 March 2020
© Springer-Verlag GmbH Austria, part of Springer Nature 2020

Abstract

It is of great significance to obtain the high precise structural surface properties of rock mass during the process of deep geotechnical engineering investigation by in-situ instrumentation, especially for preventing disasters and reducing damages. To obtain more detailed features of the structural surface in the image obtained by digital panoramic borehole imaging technique, this paper describes and analyzes the morphological feature of structural surface in the borehole image during in-situ instrumentation, and the feature is used to describe joint roughness coefficient (JRC) and analyzed the anti-sliding ability of borehole rock mass. We use a digital panoramic borehole imaging system to obtain the camera image and related data of borehole rock mass, extract the profile line of structural surface in the image, analyze the dip direction and dip angle, and transform the circular profile line of structural surface into three-dimensional feature. Finally, the statistical parameters of three-dimensional feature from the profile lines in each direction are calculated and used to form a roughness coefficient rose diagram according to related JRC theory. Results show that the rose diagram can well describe the actual three-dimensional morphology of the structural surface and its anisotropy of borehole rock mass structures. This paper provides a novel way to describe the morphological feature of structural surface in borehole image and can be applied to determine the dominant anti-slip direction of rock structure, which can solve the difficulty of obtaining the morphological features and mechanical properties of structural surface in deep rock mass.

Keywords Digital panoramic borehole imaging · Structural surface · Morphological feature · In-situ instrumentation · Joint roughness coefficient · Dominant anti-slip direction

1 Introduction

The study of structural surfaces in the borehole image is the basic work of engineering geological investigation by in-situ instrumentation. Numerous studies and tests have shown that the mechanical properties of rock structure are not only related to the characteristics of rock mass and the combined state of structural surface, but also are affected by the morphological feature of the structural surface. For a hard-structural surface with low filling degree, the surface morphology of the structural surface is the main influencing factor, which is controlling the mechanical properties of the structural surface (Bae et al. 2011; Luo et al. 2016). Therefore, the description and classification of rock surface have a vital significant for mechanical properties of rock mass. At present, some techniques related to laser profilometry and mathematical morphology are widely used to describe the morphological structures of rock surfaces, and have developed many

✉ Xianjian Zou
xjzou@whrsm.ac.cn

✉ Huan Song
songhuan@whu.edu.cn

¹ State Key Laboratory of Geo-Mechanics and Geotechnical Engineering, Institute of Rock and Soil Mechanics, Chinese Academy of Sciences, Wuhan 430071, Hubei, People's Republic of China

² Innovation Academy for Precision Measurement Science and Technology, Chinese Academy of Sciences, Wuhan 430077, Hubei, People's Republic of China

³ Department of Electrical Computer and Energy Engineering, University of Colorado Boulder, Boulder, CO 80309-0425, USA

⁴ University of Chinese Academy of Sciences, Beijing 100049, People's Republic of China

⁵ Electronic Information School, Wuhan University, Wuhan 430072, Hubei, People's Republic of China

kinds of introsopic camera system used in boreholes (Młynarczyk 2010; Młynarczyk et al. 2016; Skoczylas and Godyń 2014), which have promoted the development and progress of rock and soil mechanics. However, obtaining information on deep structural surface in the borehole image by drilling and coring has many limitations. First, due to the rotational displacement of the core during the core drilling process, the occurrence information of structural surface in the borehole image may have been destroyed. Second, some disturbances generated by high-speed rotation of the drill bit and the circulation of the drilling fluid in the coring tube may affect the determination of openness and filling for the structural surface (Li et al. 2017; Valdez et al. 2018). Therefore, using the core as the source of structural surface information may exist some errors because of above uncontrollable influencing factors. It is necessary to propose an in-situ instrumentation technique to directly measure the structural surface of the drilled hole and obtain the morphological information of structural surface in the borehole image using in-situ instrumentation technique.

Digital panoramic borehole imaging technique and its related camera system are widely applied for in-situ instrumentation in recent year (Wang et al. 2017; Zou et al. 2018). It can obtain the camera image of borehole rock mass directly and the occurrence information of in-situ structural surface on the borehole wall. The obtained image and related occurrence information of rock hole wall are accurate and reliable without the effect of the core drilling process. Therefore, using an in-situ instrumentation technique, that is digital panoramic borehole imaging technique, can be more accurate in theory and will be more meaningful by in-situ instrumentation (Bae et al. 2011; Hashemi et al. 2015; Wang et al. 2018; Winkler and D'Angelo 2006; Zhang et al. 2010). There is great significance for the research of mechanical property based on in-situ camera image of borehole rock mass using digital panoramic borehole imaging technique.

This paper uses digital panoramic borehole imaging technique to obtain the camera image and related data, that is, the borehole image of hole-wall rock mass during in-situ instrumentation, and then extracts the profile line of structural surface, analyzes the dip direction and the dip angle, and transforms the circular structural profile line into three-dimensional feature. According to the relationship between three-dimensional feature of the profile line on the structural surface and related joint roughness coefficient (JRC) theory, the feature parameters of the profile lines in each direction are calculated, and they are used to form roughness coefficient rose diagram. Finally, the rose diagram with different parameters of the profile line is used to analyze some mechanical properties of the structural surface in deep borehole rock mass.

2 Analysis of Borehole Images

The digital panoramic borehole imaging technique is based on the principle of optical imaging. It uses panoramic technology to achieve the simultaneous observation of 360° hole walls, directly providing hole-wall images by photos or videos, and then, the relevant data and borehole image can be obtained accurately and further be engaged in quantitative analysis (Wang et al. 2016).

2.1 Image Resolution Analysis

The borehole image is composed of dot matrix pixels; that is, the minimum unit is composed of pixels. Therefore, it is necessary to analyze the correspondence between the image pixels and the actual size of the observed point on the hole wall.

Using the diameter of diamond drill bit as a benchmark, the circumferential image resolution and axial image resolution can be expressed as Eqs. (1) and (2):

$$\mu_v = \frac{2\pi D_\emptyset}{n_v}, \quad (1)$$

$$\mu_h = \frac{H_z}{n_h}, \quad (2)$$

where μ_v is the circumferential image resolution; n_v is the number of circumferential pixel points of the hole-wall image; D_\emptyset is the borehole wall diameter ($D_\emptyset = 46$ mm, 59 mm, 75 mm, 91 mm, 110 mm, 130 mm); μ_h is the axis image resolution; n_h is the number of axial pixel points of the borehole wall image; H_z is the actual measurement distance along the borehole.

Assuming a digital borehole camera system with the lowest sampling capability, the axial image resolution obtained by the borehole camera system is 0.2 mm/pixel according to the specification and design principle of the system. The circumferential image resolution is related to the borehole diameter. Borehole images obtained by different diameters of the boreholes may exist different circumferential image resolution in theory. It is known that the number of pixels in the circumferential image of the borehole wall is fixed for a certain borehole camera system, such as 1024 and 2048. The circumferential image resolution corresponding to boreholes with different diameters can be shown as Fig. 1. As shown in Fig. 1, the drilling equipment with the lowest resolution sampling capability is used to measure boreholes with diameter within $= D_\emptyset 130$ mm, and the circumferential image resolution of borehole images can be less than 0.5 mm/pixel, which can basically meet the sampling analysis resolution requirements of structural surface in the borehole.

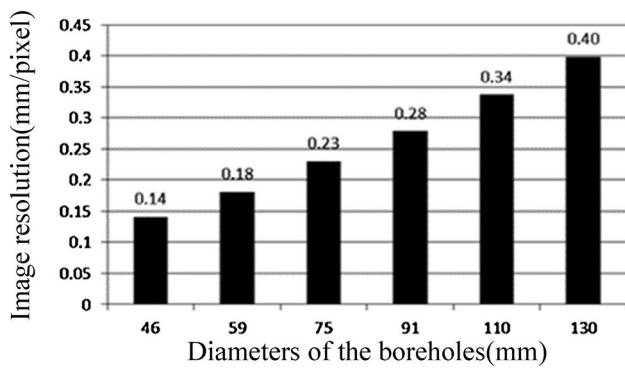
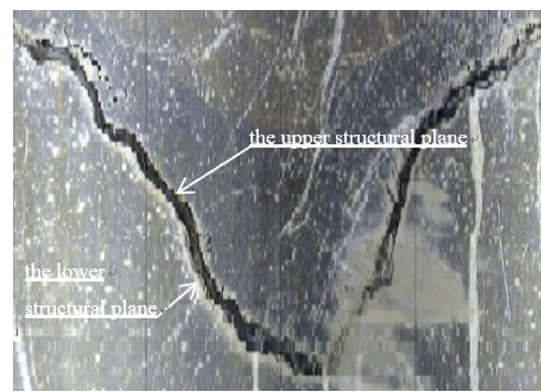


Fig. 1 Relationship between borehole diameter and circumferential image resolution



17 / 21

Fig. 3 Structural surface in borehole image from a borehole with 91 mm diameter

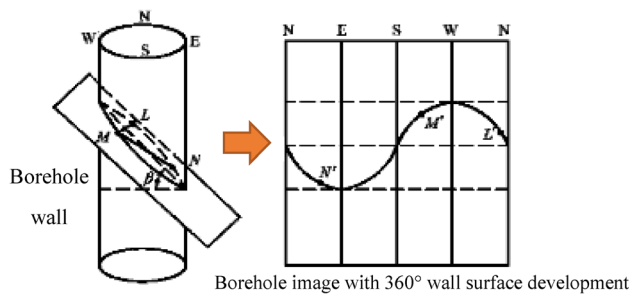


Fig. 2 Curve of structural surface in the borehole image

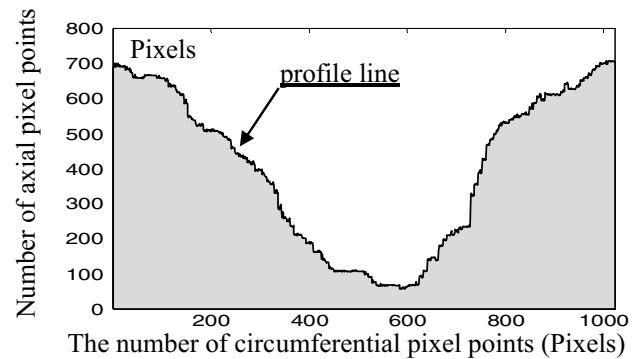


Fig. 4 Profile line of the lower structural surface in borehole image

2.2 Extract the Profile Line of Structural Surface

Digital panoramic borehole imaging technique can accurately observe the image of the 360° hole wall at any depths, and then transform the hole-wall image into borehole image with 360° wall surface development. If the structural surface is an ideal smooth surface to completely cut the borehole, it will show a continuous sinusoidal curve on the borehole image with 360° wall surface development (Zou et al. 2017), as shown in Fig. 2.

The north of borehole wall is shown on the left side of the borehole image, the β is the dip angle of structural surface, and some feature points M , N , and L in the borehole wall are shown as in points M' , N' and L' in the borehole image. However, the curve of structural surface in the actual borehole image is not smooth and it is anisotropic morphology. If the borehole is cut by the same morphology surface, it will leave a rough profile line on the borehole image, as shown in Fig. 3.

From Fig. 3, the structural surface in the borehole image can be divided into two parts: the upper structural surface and the lower structural surface in the borehole image. The upper and lower structural surface intersects with the borehole wall to form two profile lines. Taking the lower

structural surface in Fig. 3 as an example, the digital image edge detection technique can be used to extract the profile lines. We take an improved Canny method (Mokrzycki and Samko 2012; Panetta et al. 2011) to detect the edge of structural surface and lastly obtained profile line of the lower structural surface is shown in Fig. 4. It can be clearly seen that the profile line of the lower structural surface in borehole image is like the sinusoidal curve just with a different phase.

2.3 Transform the Spatial Position of the Profile Line

Structural surfaces in borehole image have many morphological and physical characteristics, which can be represented by the hues, shapes, and widths of the sinusoidal ribbons. The intersections of structural surfaces in the borehole are approximately ellipses in the three-dimensional space, which become sine curves when expanded onto a two-dimensional image (Assous et al. 2013; Glossop et al. 1999; Thapa et al. 1997; Wu et al. 2011).

Therefore, the ideal intersection between the smooth surface and the borehole wall is an ideal sinusoidal curve. The occurrence information of structural surface can be calculated based on the amplitude and phase of the sinusoidal curve in the borehole image. Combined with the measured drilling depth, the structural surface spatial position information can be obtained.

Therefore, the general equation of sinusoidal curve can be used to fit the profile line. The general equation of sinusoidal curve is Eq. (3):

$$y = A \cdot \sin(\omega \cdot x + \varphi) + k, \tag{3}$$

where A is the amplitude; ω is the angular velocity, which controls the period of sinusoidal curve; φ is the initial phase, reflected lateral displacement in the x - y coordinate system; k is the offset distance, reflected longitudinal displacement in the x - y coordinate system.

According to the least-squares fitting principle, the optimal criterion value f can be set as:

$$f = \sum_{i=1}^N [Y(x) - y(x)]^2 = \sum_{i=1}^N [Y(x) - (A \cdot \sin(\omega \cdot x + \varphi) + k)]^2, \tag{4}$$

where f is the optimal criterion value; N is the total number of sample points, that is, the number of circumferential pixel points of the borehole image (1024); $Y(x)$ is the ordinate value of the point on the profile line; $y(x)$ is the ordinate value of the point on the sinusoidal curve.

Because the circumferential image resolution μ_v is not equal to the axis image resolution μ_h , the coordinate system of image in Fig. 4 needs to be corrected and transformed into actual length coordinate system. Therefore, the horizontal and vertical coordinates of profile line are, respectively, multiplied by the corresponding image resolution to obtain the actual length of profile line, as shown in Fig. 5. Using the optimal criterion value f as constraint condition to fit the obtained profile line in Fig. 4, the fitting sinusoidal curve can be obtained and shown in Fig. 5.

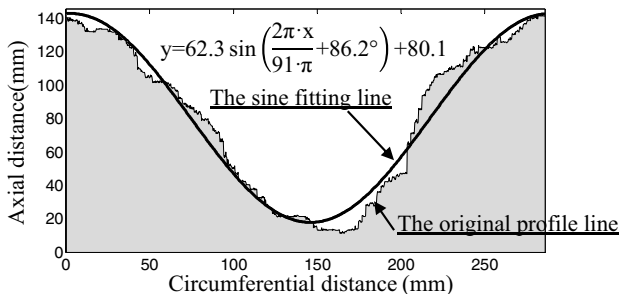


Fig. 5 Sine fitting line of sinusoidal curve and the actual obtained profile line

According to the general equation of sinusoidal curve, the surface represented by the sine fitting line can be calculated. The represented surface is the closest surface to the lower structural surface in borehole wall. Therefore, it can be regarded as the reference surface. The occurrence information of the structural surface can be represented by the occurrence of the reference surface, and then, the occurrence of the reference surface can be obtained from the parameters of the sinusoidal curve general equation. The left of the sine fitting line in the image (Fig. 5) represents the true north direction, so the dip direction θ of the reference surface is:

$$\theta = 270^\circ - \varphi = 183.8^\circ. \tag{5}$$

The dip angle β is:

$$\beta = \arctan\left(\frac{2A}{D}\right) = 53.9^\circ. \tag{6}$$

3 Analysis of Profile Line of Structural Surface

The profile line of the structural surface in borehole image which obtained from borehole wall is not in the vertical direction of structural surface. Therefore, the coordinate and visual distance of the profile line based on the reference surface should be transformed before analysis.

First, the sine fitting line is used as a reference and expanded into a straight line, and then, the coordinate of the profile line is transformed along with the sine fitting line. According to the results in Fig. 5, a certain square block is intercepted, as shown in Fig. 6. Create an x' - y' coordinate system on the sine fitting line, use the intersection of the y -axis and the sine fitting line in Fig. 5 as the origin of coordinate, take the path of the sine fitting

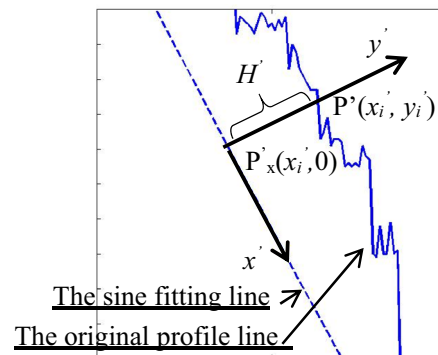


Fig. 6 Schematic diagram of transformation for a random segment in Fig. 5

line as the x' -axis, and take the vertical direction of the sine fitting line as the y' -axis. Then, the vertical distance from the point on the profile line to the sine fitting line in borehole image is H_i .

In the x - y coordinate system of Fig. 5, the point on the profile line in the true north direction is taken as the starting point and other points are numbered in the clockwise direction. The coordinate of the i th point P on the profile line is (x_i, y_i) , which is corresponding to $P'(x'_i, y'_i)$ in the x' - y' coordinate. The projection of point P' on the x' -axis is $P'_x(x'_i, 0)$ and P'_x corresponds to $P_x(x_j, y_j)$ in the x - y coordinate. Then, the relationship between point P and point P_x coordinate can be shown as Eq. (7):

$$P(x_i, y_i) = \begin{cases} \text{The profile line} \\ y = \frac{-1(x-x_j)}{A\omega \cos(\omega x + \varphi)} + A \sin(\omega x + \varphi) + k. \end{cases} \quad (7)$$

The linear distance of H_i between P and P_x can be shown as Eq. (8):

$$H_i = \sqrt{(x_i - y_j)^2 + (x_i - y_j)^2}. \quad (8)$$

Then, the calculated value H_i according to Eq. (8) also requires a line-of-sight transformation. There is an angle between the structural surface and the reference surface for the borehole wall, and most of them are oblique crossing and shown in Fig. 7. A line-of-sight transformation should be taken to obtain the vertical distance from the profile line to the reference surface.

Random point P on the profile line and its foot of a perpendicular P_x on the sine fitting line in Fig. 6 correspond to P_1, P_2 and P_{x1}, P_{x2} in Fig. 7. The known line segment ($\overline{PP_x}$) is perpendicular to the line of intersection between the reference surface and the borehole wall at the P_x point. However, $\overline{PP_x}$ is not perpendicular to the reference

surface, and the angle between the reference surface and the borehole wall at P_{x1} is not equal to the angle between the reference surface and the borehole wall at P_{x2} as shown in Fig. 7. Therefore, the line-of-sight transformation of the calculated value H_i in Eq. (8) is:

$$H'_i = H_i \cdot \cos \alpha_i, \quad (9)$$

where H'_i is the vertical distance from point P to the reference surface at random point on the profile line; α_i is the angle between the reference surface and the horizontal direction in the projection of $\overline{PP_x}$, and the α_i is calculated by Eq. (10):

$$\alpha_i = a \tan \left(\frac{|2A \cdot \sin(\omega \cdot x_j + \varphi)|}{D} \right). \quad (10)$$

According to Eqs. (7)–(10) and coordinate transformation relationship, the corresponding relationship between any point $P'(x'_i, y'_i)$ in the x' - y' coordinate system and point $P_x(x_i, y_j)$ in the x - y coordinate system can be obtained as follows:

$$x'_i = \int_0^x \sqrt{1 + [A \cdot \omega \cdot \cos(\omega \cdot x_j + \varphi)]^2} dx, \quad (11)$$

$$y'_i = H'_i. \quad (12)$$

Another, because the profile line is the curve around the borehole wall, all the points on the profile line have azimuth information, which can be reflected in the x' - y' coordinate system at the same time; that is, the azimuth information of the points on the profile line corresponds to the coordinate value of the x' -axis. The corresponding relationship is shown as Eq. (13):

$$\gamma'_i = \frac{360^\circ}{\mu_v} \cdot i, \quad (13)$$

where γ'_i is azimuth of i th point.

According to the above coordinate transform relationship, a development diagram of the profile line in the direction of the sine fitting line can be obtained. The x -axis is the circumferential distance along with the sine fitting line, and the azimuth information of the point on the profile line corresponds to the x -axis. The y -axis is the vertical distance of the profile line to the reference surface, and the origin is 0° in the sine fitting line. Taking the profile line of the structural surface in Fig. 5 as an example, the profile line is developed in Fig. 8.

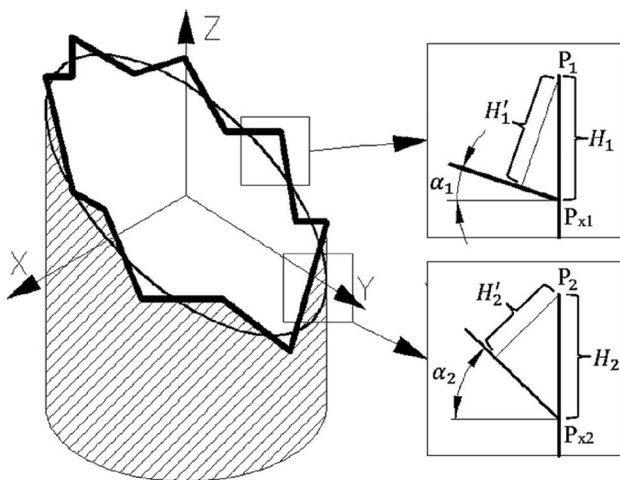
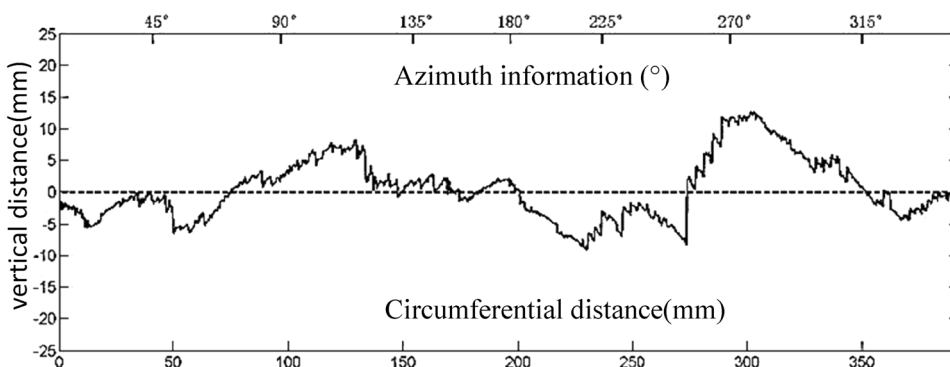


Fig. 7 Oblique-crossing structural surface and borehole wall

Fig. 8 Development diagram of the profile line in the direction of the sine fitting line



4 Morphological Feature Description Method

The roughness of rock fracture surface can be reflected by the fractal dimension. When the size scale of measure is fixed, the larger the fractal dimension is, the rougher the fracture surface is, which can quantitatively reflect the morphological features of the structural surface in the obtained borehole image (Alameda-Hernandez et al. 2014; Xie et al. 1998; Zhou and Xie 2003).

4.1 Analysis of Sampling Length and Sampling Resolution

The profile line in different directions of the structural surface has different morphological features, so it is necessary to find a suitable parameter to quantify the differences between different morphological features. Fractal dimensions are used to characterize the anisotropy of the profile lines from fracture surfaces and joint segments (Alameda-Hernandez et al. 2014; Li and Huang 2015). Referring to the previous work, we obtain the fractal dimension of the profile line in Fig. 8 and use it to describe the anisotropic characteristics of the structural surface.

To ensure that the calculated fractal dimension is comparable between different segment profiles, it is necessary to discuss the sampling length and sampling resolution of each segment profile. It is known that the profile line of the structural surface in Fig. 5 is in the form of an approximately sinusoidal curve, and the borehole image just has equal interval sampling characteristics in horizontal and vertical directions. Therefore, the development diagram (Fig. 8) of the profile line along with the direction of the sine fitting line does not have the property of equal spacing between sampling points, and the greater dip angle of the structural surface, the more obvious difference of the profile line in sampling resolution between different profile lines.

The sampling resolution is represented by the sampling step distance Δr , and the sampling step Δr between random two sampling points is calculated as Eq. (14):

$$\Delta r = \int_{x_0}^{x_0+\Delta r} \sqrt{1 + [A \cdot \omega \cdot \cos(\omega \cdot x + \varphi)]^2} dx, \tag{14}$$

where Δr is the sampling step; x_0 is the abscissa of random point on the profile line in development diagram (Fig. 8).

By comparing the profile line with different sampling lengths, some results show that the sampling steps between the sampling points in the same segment have a small difference, and the maximum step difference is less than 10% when the sampling length of the profile line is less than 15 mm. Therefore, the sampling point can be approximated as equally spaced sample when the sampling length is less than 15 mm.

When the profile line segment approximately satisfies the equal space sampling, the difference in the sampling resolution between segments will also affect the calculation of the fractal dimension. The maximum difference between the sampling steps between segments is:

$$\Delta R_{\max} = 1 \cdot \left(\frac{\mu_v}{\cos \beta} - \mu_v \right), \tag{15}$$

where ΔR_{\max} is the maximum difference between the sampling steps. When $\beta < 60^\circ$, $\Delta R_{\max} < 1 \cdot \mu_v$.

When the sampling step distance is within 0.125 mm ~ 1 mm, the fractal dimensions of the profile line can be calculated from different sampling step length and sampling length (Wang et al. 2000) as shown in Fig. 9. From Fig. 9, it can be clearly seen that the fractal dimension has been affected by the sampling length and the sampling step size, showing a significant scale effect, when the fractal dimension of the sampling length within 50 mm.

In summary, to ensure that the calculated fractal dimension is comparable between different segment profiles, the same sampling length and sampling resolution are required in different segments of the profile line and it is necessary to unify the profile lines. To ensure that the sampling data are reliable, a linear interpolation method is used to simplify the profile lines and reduce the sampling resolution between

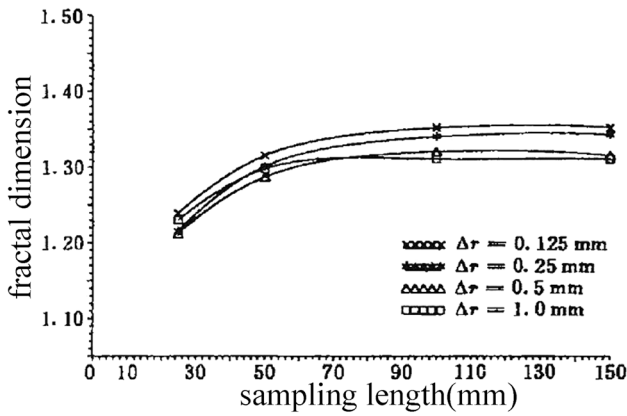


Fig. 9 Scale effect of fractal dimension D from different rock fracture profiles

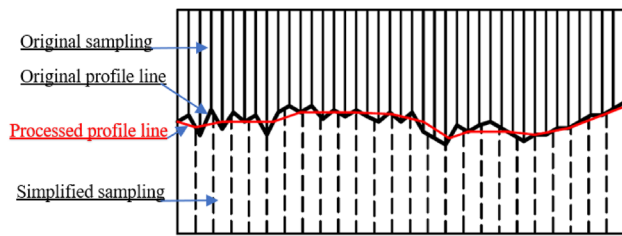


Fig. 10 Simplify treatment for a segment of the profile line

the sampling points, so that different profile line segments have the same sampling resolution, just as shown in Fig. 10.

4.2 Morphological Feature Description Method

On the reference plane, the tangent line of the sine fitting line of the profile line is made. The central point is the point of tangent corresponding to the profile line, and a segment (length L) of the profile line is taken. When the vector direction of the approximate normal of the segment changes δ each time, sub-segment is cut off once, and then, sub-segment ($360^\circ/\delta$) can be obtained. Then, the profile line is treated uniformly, and the fractal dimension of each segment is calculated separately.

Taking the influence of the meso-structure of the rock material into account, the fluctuation degree of rough body on the rock surface shows a certain correlation with the position within a certain range. Therefore, the self-affine fractal description method which, like the Brownian motion process, can be used (Cambonie et al. 2015). According to the data characteristics of the sampling points on the segment of profile line, the fractal dimension calculation is as follows:

Let the vertical distance H'_i from any point P on the profile segment to the reference plane be a random variable, and calculate the mean square error function $V(n)$ of the

profile segment. The $V(n)$ of self-affine fractal properties is expressed in the form of explicit function Eq. (16) or Eq. (17):

$$V(n) = \frac{1}{N' - n + 1} \sum_{i=1}^{N'-n+1} [H'_{i+n} - H'_i]^2 = B \cdot [\Delta l]^{2(2-D)}, \tag{16}$$

or

$$V(n) = \frac{1}{N' - n + 1} \sum_{i=1}^{N'-n+1} [H'_{i+n-1} - H'_i]^2 = B \cdot [\Delta r \cdot (n - 1)]^{2(2-D)}, \tag{17}$$

where $V(n)$ is the mean square error function; N' is the total number of sample points in the total sample; n is the total number of sample points in the sub-sample; B is the coefficient; D is the fractal dimension; Δl is the length of the sub-sample, and $\Delta l = \Delta r \cdot (n - 1)$ for equally spaced sampling. Therefore, let us take the logarithm of the equal sign in Eq. (16) and simplified as:

$$D = 2 - \frac{\ln V(n) - \ln B}{2 \ln [\Delta l]}. \tag{18}$$

Take,

$$\varepsilon = \frac{\ln V(n) - \ln B}{\ln [\Delta l]}. \tag{19}$$

Then, we can get:

$$\ln V(n) = \ln B + \varepsilon \cdot \ln \Delta l. \tag{20}$$

Obviously, ε is its slope, and $\ln B$ is the intercept on the $\ln V(n)$ axis in the logarithmic relationship between $V(n)$ and Δl .

Brownian motion is a typical example of fractal theory, and the Brownian motion under ideal state is Gaussian normal distribution (Babadagli and Develi 2001), so the fitting result obtained by the least-square method is the optimal linear unbiased estimator; that is, it has the smallest variance among all linear unbiased estimations according to related theoretical analysis (Valdez et al. 2018).

Take the profile line of structural surface, the sine fitting line, and the reference surface in Fig. 5 as example, set $L = 30$ mm, $\delta = 10^\circ$, and then, the profile line is divided into 36 segments. After simplifying treatment, the profile segments with equal spaced sampling are obtained. The mean square error $V(n)$ of profile segment was calculated respectively, and the least-square method was used to fit the one-dimension function in the log-log relation diagram between $V(n)$ and Δl . Take the 0° segment of the profile line as an example, and the fitting results are shown in Fig. 11.

From Fig. 11, the slope of the fitting line of log-log relation diagram is $\varepsilon = 1.1406$, $\ln(B) = -1.1094$, and fractal dimension $D = 1.4297$ can be calculated. According to the

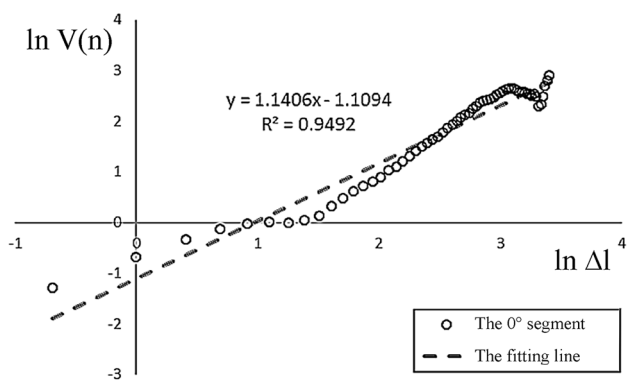


Fig. 11 Log–log relation diagram of $V(n)$ and Δl , and the fitting line of the log–log relation from the 0° segment of the profile line

calculation formula of mean square error $V(n)$ of the profile segment, it can be seen that when the sub-sample length Δl is larger, the data utilization rate of the sampling point on the profile segment is lower, which is reflected in the fact that the log–log relationship between $V(n)$ and Δl is more sensitive and prone to distortion. Similarly, the logarithmic relationship between $V(n)$ and Δl is no longer linearly correlated near the maximum value of Δl according to the marked position of the dotted line circle in Fig. 11.

Therefore, when calculating the fractal dimension of the 36-segmented profile line on the structural surface in the same way, some logarithm values of $V(n)$ and Δl near the maximum value are first removed to make the linear correlation coefficient of the linear fitting results greater than 0.9 ($R^2 \geq 0.81$). Finally, the calculated results are displayed using the rose diagrams, and the fractal dimension rose diagram can be used to approximate describe the three-dimensional morphological features of the structure plane. The results are shown in Fig. 12.

Figure 12 shows that the fractal dimension is symmetric in the circumferential direction of the structural surface in

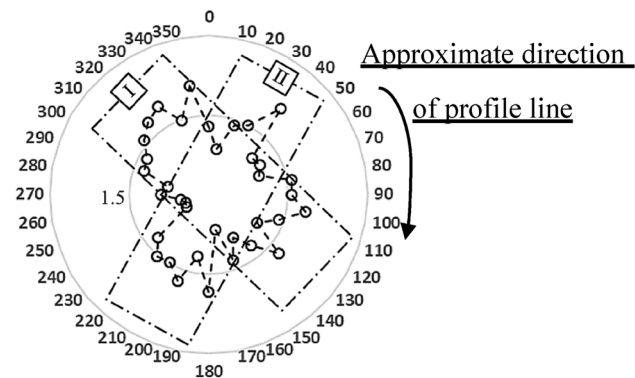


Fig. 12 Rose diagram with fractal dimensions from the statistical results of circumferential profile segments of the structural surface

the borehole image, which is significantly reflected in the two rectangular marks I and II. Therefore, it is judged that there is a symmetrical distribution of the morphological feature of profile line segments on the structural surface; that is, the symmetrical distribution of mechanical properties can be obtained by morphological feature description method of structural surface in borehole image.

5 Application in JRC Value Description

At present, the JRC values are generally determined by comparison with Barton’s proposed ten standard profile lines, and there are some scholars who indirectly determined the JRC values of rock surface based on the statistical parameters of the rock profile lines and fractal theory. This application is based on the borehole image obtained from the digital panoramic borehole imaging system, and then calculate JRC values according to above morphological feature description method. Finally, we make a JRC rose diagram to express the morphological feature description results of structural surface in borehole image during in-situ instrumentation.

To meet the requirements of applying the relationship between JRC value and fractal dimension D , and the corresponding relationship between JRC value and statistical parameters of rock surface, it is necessary to process the micro-texture of rock structural surface and remove some micro-morphology features. Taking the profile line of the structural surface in Fig. 5 as an example, the microscopic morphology of the profile line is in a clear zigzag shape, which will inevitably cause interference when the surface parameters are counted or the fractal dimension is calculated. Therefore, it is necessary to remove the micro-zigzag texture of the profile line of the surface in advance and retain its macro-roughness morphology. The profile line segment (length 10 cm) has been removed the micro-zigzag texture by in a cubic interpolation, as shown in Fig. 13.

The profile line of the structural surface after removing the micro-zigzag texture is like that of N. Barton’s 10 standard curves, so the fractal dimension or surface roughness statistical parameter of the profile line can be calculated, and then, the JRC value can be obtained by the corresponding relationship of JRC according to some researchers’

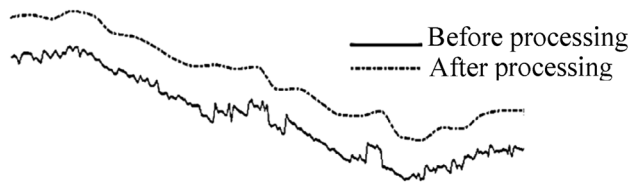
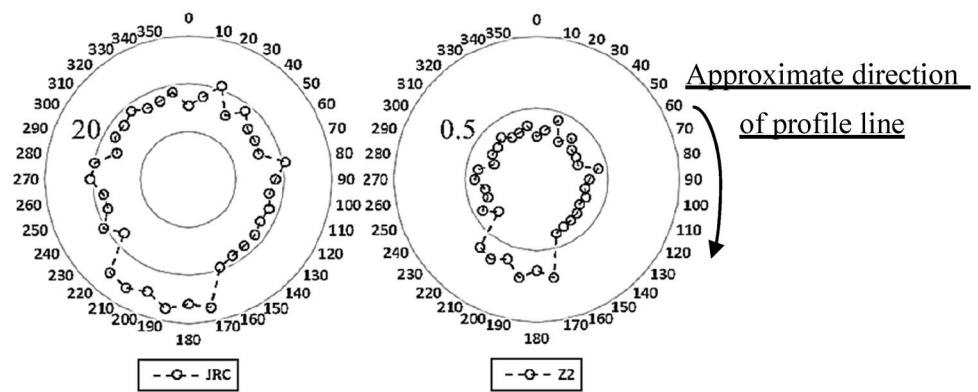


Fig. 13 Processing of micro-zigzag texture in the profile line of the surface

Fig. 14 Rose diagram with statistical parameters Z_2 and JRC values



publications, such as (Babanouri and Nasab 2017; Babanouri et al. 2013).

The ten standard curves of N . Barton were calculated and found that there are two statistical parameters with the highest degree of correlation between the JRC and the root mean square (RMS) (Tse and Cruden 1979). The corresponding relationship between the JRC and the statistical parameter Z_2 can be shown as:

$$JRC = 32.2 + 32.47 \log Z_2, \tag{21}$$

$$Z_2 \approx \sqrt{\frac{1}{L} \sum_{i=1}^{N-1} \frac{(H'_{i+1} - H'_i)^2}{x'_{i+1} - x'_i}}, \tag{22}$$

where N is the number of sampling points; L is the total sampling length.

Still taking the profile line of structural surface in the borehole image, the sine fitting line, and the reference surface in Fig. 5 as example, set the interception length $L=100$ mm of the profile line, the sampling rate $\delta = 10^\circ$, and then, we can get 36 segments of the profile line. After eliminate the surface micro-structure characteristics of these segments, statistical parameters Z_2 and JRC values of every segment are calculated separately, and then, the Z_2 and JRC values are drawn into the rose diagram respectively, just as shown in Fig. 14.

From Fig. 14, there is an obvious phenomenon that the roughness increases together significantly in the sampling area of $180^\circ-220^\circ$, so it is judged that the anti-sliding ability of the rock mass in the direction of $180^\circ-220^\circ$ is better than that in other directions. Therefore, the dominant anti-slip direction of the structural surface can be determined as about 200° in Fig. 14.

6 Conclusions

This paper proposes a method to describe the morphological features of structural surface in borehole image using digital panoramic borehole imaging technique, and forms a fractal dimension rose diagram to show the three-dimensional morphological features of the structural surface borehole rock mass. From the perspective of the macroscopic statistical analysis of the entire borehole, the occurrence and spatial distribution of structural surfaces in borehole image can be accurately obtained using the morphological feature description method. From the view of microscopic statistical point of each structural surface, the analysis of the profile line can be performed at a higher sampling resolution to identify the morphological features of the structural surface in borehole rock mass.

Therefore, using the digital panoramic borehole imaging system as an in-situ instrumentation technique to obtain the morphological feature of structural surface in borehole rock mass is feasible. The rose diagram with fractal dimension can well show the three-dimensional roughness information of structural surface in borehole and the symmetrical distribution of rock mass mechanical properties, and also the anisotropy of surface morphological features. Another, the rose diagram with JRC values can be used to determine the dominant anti-slip direction of the structural surface in borehole rock mass according to the relationship between the morphological feature and the mechanical properties of the structural plane in the obtained borehole image, which can solve the difficulty of obtaining the three-dimensional morphological features information and the mechanical properties of structural surface in deep rock mass.

Acknowledgements This work was supported by the Key Project of Natural Science Foundation of China (No. 41731284) and the Natural Science Foundation of Hubei (2019CFB345). This paper has no conflict of interest.

Compliance with Ethical Standards

Conflict of interest The authors declare that they have no conflict of interest.

References

- Alameda-Hernandez P, Jimenez-Peralvarez J, Palenzuela JA, El Hamdouni R, Irigaray C, Cabrerizo MA, Chacon J (2014) Improvement of the JRC calculation using different parameters obtained through a new survey method applied to rock discontinuities. *Rock Mech Rock Eng* 47:2047–2060. <https://doi.org/10.1007/s00603-013-0532-2>
- Assous S, Elkington P, Clark S, Whetton J (2013) Automated detection of planar geologic features in borehole images. *Geophysics* 79:D11–D19
- Babadagli T, Develi K (2001) On the application of methods used to calculate the fractal dimension of fracture surfaces. *Fractals* 9:105–128. <https://doi.org/10.1142/s0218348x01000464>
- Babanouri N, Nasab SK (2017) Proposing triangulation-based measures for rock fracture roughness. *Rock Mech Rock Eng* 50:1055–1061. <https://doi.org/10.1007/s00603-016-1139-1>
- Babanouri N, Nasab SK, Sarafrazi S (2013) A hybrid particle swarm optimization and multi-layer perceptron algorithm for bivariate fractal analysis of rock fractures roughness. *Int J Rock Mech Min Sci* 60:66–74
- Bae D-s, Kim K-s, Koh Y-k, Kim J-y (2011) Characterization of joint roughness in granite by applying the scan circle technique to images from a borehole televiewer. *Rock Mech Rock Eng* 44:497–504
- Cambonie T, Bares J, Hattali ML, Bonamy D, Lazarus V, Auradou H (2015) Effect of the porosity on the fracture surface roughness of sintered materials: From anisotropic to isotropic self-affine scaling. *Phys Rev E*. <https://doi.org/10.1103/PhysRevE.91.012406>
- Glossop K, Lisboa PJ, Russell PC, Siddans A, Jones GR (1999) An implementation of the Hough transformation for the identification and labelling of fixed period sinusoidal curves. *Comput Vis Image Underst* 74:96–100
- Hashemi SS, Taheri A, Melkoumian N (2015) An experimental study on the relationship between localised zones and borehole instability in poorly cemented sands. *J Petrol Sci Eng* 135:101–117. <https://doi.org/10.1016/j.petrol.2015.08.009>
- Li Y, Huang R (2015) Relationship between joint roughness coefficient and fractal dimension of rock fracture surfaces. *Int J Rock Mech Min Sci* 75:15–22. <https://doi.org/10.1016/j.ijrmms.2015.01.007>
- Li Y, Xu Q, Aydin A (2017) Uncertainties in estimating the roughness coefficient of rock fracture surfaces. *Bull Eng Geol Environ* 76:1153–1165. <https://doi.org/10.1007/s10064-016-0994-z>
- Luo S, Zhao Z, Peng H, Pu H (2016) The role of fracture surface roughness in macroscopic fluid flow and heat transfer in fractured rocks. *Int J Rock Mech Min Sci* 87:29–38. <https://doi.org/10.1016/j.ijrmms.2016.05.006>
- Młynarczuk M (2010) Description and classification of rock surfaces by means of laser profilometry and mathematical morphology. *Int J Rock Mech Min Sci* 47:138–149. <https://doi.org/10.1016/j.ijrmms.2009.09.004>
- Młynarczuk M, Habrat M, Skoczylas N (2016) The application of the automatic search for visually similar geological layers in a borehole in introsopic camera recordings. *Measurement* 85:142–151. <https://doi.org/10.1016/j.measurement.2016.02.043>
- Mokrzycki W, Samko M (2012) Canny edge detection algorithm modification. In: Bolc L, Tadeusiewicz R, Chmielewski LJ, Wojciechowski K (eds) *Computer vision and graphics*. Springer, Berlin, Heidelberg, pp 533–540
- Panetta KA, Agaian SS, Nercessian SC, Almunstashri AA (2011) Shape-dependent canny edge detector. *Opt Eng*. <https://doi.org/10.1117/1.3613941>
- Skoczylas N, Godyń K (2014) Evaluating selected lithological features using photographs taken with an introsopic camera in boreholes. *Int J Rock Mech Min Sci* 72:319–324. <https://doi.org/10.1016/j.ijrmms.2014.09.017>
- Thapa BB, Hughett P, Karasaki K (1997) Semi-automatic analysis of rock fracture orientations from borehole wall images. *Geophysics* 62:129–137
- Tse R, Cruden D (1979) Estimating joint roughness coefficients. *Int J Rock Mech Min Sci Geomech Abs* 16:303–307. [https://doi.org/10.1016/0148-9062\(79\)90241-9](https://doi.org/10.1016/0148-9062(79)90241-9)
- Valdez AV, Morel S, Marache A, Hinojosa M, Riss J (2018) Influence of fracture roughness and micro-fracturing on the mechanical response of rock joints: a discrete element approach. *Int J Fract* 213:87–105. <https://doi.org/10.1007/s10704-018-0308-5>
- Wang C, Wang Y, Han Z, Wang J, Zou X (2018) A system for measuring borehole diametric deformation based on mechanical contact and micro-optical imaging. *Measurement* 130:191–197. <https://doi.org/10.1016/j.measurement.2018.07.088>
- Wang C, Zou X, Han Z, Wang J, Wang Y (2017) The automatic interpretation of structural plane parameters in borehole camera images from drilling engineering. *J Petrol Sci Eng* 154:417–424. <https://doi.org/10.1016/j.petrol.2017.03.038>
- Wang C, Zou X, Han Z, Wang Y, Wang J (2016) An automatic recognition and parameter extraction method for structural planes in borehole image. *J Appl Geophys* 135:135–143. <https://doi.org/10.1016/j.jappgeo.2016.10.005>
- Wang JA, Xie H, Tian X (2000) Scale effect on fractal measurement of rock fracture surfaces. *Chin J Rock Mech Eng* 19:11–17
- Winkler KW, D'Angelo R (2006) Ultrasonic borehole velocity imaging. *Geophysics* 71:F25–F30. <https://doi.org/10.1190/1.2194532>
- Wu J, Feng S, Li H (2011) Study of automatically extracting structural plane parameters from borehole images. *Rock Soil Mech* 32:951–957
- Xie H, Wang J-A, Stein E (1998) Direct fractal measurement and multifractal properties of fracture surfaces. *Phys Lett A* 242:41–50
- Zhang B-X, Shi F-F, Wu X-M, Gong J-J, Zhang C-G (2010) Imaging for borehole wall by a cylindrical linear phased array. *Chin Phys Lett* 27:5. <https://doi.org/10.1088/0256-307x/27/9/094301>
- Zhou H, Xie H (2003) Direct estimation of the fractal dimensions of a fracture surface of rock. *Surf Rev Lett* 10:751–762
- Zou X, Wang C, Han Z (2018) A proposed method for estimating in-situ stress direction using panoramic stereo-pair imaging and stressed borehole geometric shapes. *Int J Rock Mech Min Sci* 104:94–99. <https://doi.org/10.1016/j.ijrmms.2018.02.010>
- Zou X, Wang C, Han Z, Wang J, Wang Y, Song H (2017) Fully automatic identifying the structural planes with panoramic images of boreholes. *Yanshilixue Yu Gongcheng Xuebao Chin J Rock Mech Eng* 36:1910–1920

Publisher's Note Springer Nature remains neutral with regard to jurisdictional claims in published maps and institutional affiliations.